PHOTONICS Research

Ultra-broadband flat-top quantum dot comb lasers

Jing-Zhi Huang,[1,2,†] Zi-Tao Ji,[3,†] Jia-Jian Chen,[1,2] Wen-Qi Wei,[4] Jia-Le Qin,[1,2] Zi-Hao Wang,[1,2,4,6] Zhi-Yuan Li,[3] Ting Wang,[1,2,4,7] Xi Xiao,[5] and Jian-Jun Zhang[1,2,4,8]

[1]Beijing National Laboratory for Condensed Matter Physics, Institute of Physics, Chinese Academy of Sciences, Beijing 100190, China
[2]Center of Materials Science and Optoelectronic Engineering, University of Chinese Academy of Sciences, Beijing 100049, China
[3]School of Physics and Optoelectronics, South China University of Technology, Guangzhou 510641, China
[4]Songshan Lake Materials Laboratory, Dongguan 523808, China
[5]National Information Optoelectronics Innovation Center, China Information and Communication Technologies Group Corporation (CICT), Wuhan 430074, China
[6]e-mail: wangzihao@iphy.ac.cn
[7]e-mail: wangting@iphy.ac.cn
[8]e-mail: jjzhang@iphy.ac.cn

Received 19 October 2021; revised 16 March 2022; accepted 17 March 2022; posted 18 March 2022 (Doc. ID 446349); published 29 April 2022

A quantum dot (QD) mode-locked laser as an active comb generator takes advantage of its small footprint, low power consumption, large optical bandwidth, and high-temperature stability, which is an ideal multi-wavelength source for applications such as datacom, optical interconnects, and LIDAR. In this work, we report a fourth-order colliding pulse mode-locked laser (CPML) based on InAs/GaAs QD gain structure, which can generate ultra-stable optical frequency combs in the O-band with 100 GHz spacing at operation temperature up to 100°C. A record-high flat-top optical comb is achieved with 3 dB optical bandwidth of 11.5 nm (20 comb lines) at 25°C. The average optical linewidth of comb lines is measured as 440 kHz. Single-channel non-return-to-zero modulation rates of 70 Gbit/s and four-level pulse amplitude modulation of 40 GBaud/s are also demonstrated. To further extend the comb bandwidth, an array of QD-CPMLs driven at separate temperatures is proposed to achieve 36 nm optical bandwidth (containing 60 comb lines with 100 GHz mode spacing), capable of a total transmission capacity of 4.8 Tbit/s. The demonstrated results show the feasibility of using the QD-CPML as a desirable broadband comb source to build future large-bandwidth and power-efficient optical interconnects.

https://doi.org/10.1364/PRJ.446349

1. INTRODUCTION

The generation of optical frequency combs (OFCs) has been of great interest recently as they can provide equidistant mutually locked coherent modes, which make them ideal sources for precision metrology, data communications, and optical interconnects. Over the past decades, various approaches have been extensively investigated to realize on-chip OFCs, such as IM/phase EO modulation [1–3], soliton microresonators [4–6], gain-switched combs [7,8], and passive mode-locked lasers (MLLs) [9]. Among them, soliton microresonators have drawn significant attention recently due to their compactness and ultra-wide bandwidth. In comparison, semiconductor MLLs have the advantages of being electrically driven, while not requiring external high-power optical pumping, which makes them a great candidate for highly efficient, small-footprint, and low power consumption solutions for optical time-division multiplexing [10] and wavelength-division multiplexing (WDM) systems [11]. In recent years, there has been significant attention paid to quantum dash (Q-dash) [12–14] and quantum dot (QD) MLLs [9,15,16] as flat-top comb sources, due to their properties of small linewidth enhancement factor, fast carrier dynamic-induced self-frequency modulation, and defect insensitivity, which make them an ideal platform for a reflection insensitive [17,18], temperature insensitive [19,20], and most importantly, direct-grown-on-Si light source [21–26].

Conventionally, semiconductor MLLs have been investigated to produce the optical pulses with a wide range of repetition rates from megahertz to hundreds of gigahertz as listed in Table 1. The ultra-dense optical combs (repetition rate < 1 GHz) lead to applications for sensing or spectroscopy [27]; however, for WDM communication applications, small repetition rate, which also corresponds to narrow channel spacing of the WDM system, is limiting the highest modulation bandwidth of each channel due to strong cross talk [35]. Currently, the minimum channel spacing requirement of CW-WDM multi-source agreement (MSA) [36] is 100 GHz.

Table 1. Comparison of Mode-Locked Comb Laser on Various Material Platforms and Structures

	Mode-Locking Mode	Material Platform	Repetition Rate (GHz)	Optical Bandwidth (nm)	Optical Linewidth (kHz)	Operating Temp. (°C)
[27]	Anti-CPM (external cavity)	InGaAsP MQW on Si	1	12 (–10 dB BW)	400	20
[27]	Hybrid anti-CPM (external cavity)	InGaAsP MQW on Si	1	13 (–10 dB BW)	400	20
[28]	CPM (external cavity)	InGaAsP MQW on Si	10	6.4 (–3 dB BW)	>15	16
[29]	CPM (external cavity)	MQW on Si	20	2.96 (–3 dB BW)	NA	NA
[30]	Two-section	InAs/GaAs QD on Si	20	6.1 (–3 dB BW)	10,000	18
[31]	Two-section	InAs/GaAs QD	25.5	4.7 (–6 dB BW)	NA	20–120
[32]	Two-section	AlGaInAs/InP MQW	100	8.05 (–3 dB BW)	NA	20
[33]	CPM (external cavity)	InAs/GaAs QD on SOI	102	6.5 (–3 dB BW)	NA	25
[34]	CPM (external cavity)	InAs/GaAs QD on SOI	15.5	12 (–3 dB BW)	NA	23
This work	**Fourth-order CPM**	**InAs/GaAs QD**	**100**	**11.5 (–3 dB BW)**	**440**	**25–100**

Considering that the typically used non-return-to-zero (NRZ) modulation speed nowadays is around 100 Gbit/s, MLLs with at least 100 GHz mode spacing are required for large bandwidth data transmission. The bandwidth of flat-top OFCs is another figure of merit for the WDM system which is strongly dependent on the 3 dB optical bandwidth. It is suggested that QD MLLs have larger 3 dB bandwidth compared with the quantum well (QW) systems due to their physical nature of broad gain spectrum [9,37].

In this work, we experimentally demonstrate an O-band 100 GHz InAs/GaAs QD-colliding pulse mode-locked laser (CPML) (fourth order) with a record wide 3 dB optical bandwidth of 11.5 nm and a state-of-the-art working temperature ranging from 20°C to 100°C. By optimizing the operation conditions, we have achieved steady flat-top ML region of 20 comb lines within 3 dB optical bandwidth at 100 GHz mode spacing. The individual comb lines exhibit narrow average optical linewidth of 440 kHz. The measured relative intensity noise of the entire comb spectrum and each channel is –160 and –133 dB/Hz in the frequency range from 10 MHz to 20 GHz, respectively. The MLLs have also shown reasonable over-time wavelength drifting of approximately 200 MHz and 1 GHz for 10 min and 20 h stability examinations. The high-speed large-signal modulation experiment has been performed on each of 20 comb lines, while open eyes are obtained for both 70 Gbit/s NRZ and 40 GBaud/s four-level pulse amplitude modulation (PAM-4) modulation rates, which indicate the QD-CPML has the capability to transmit at 1.6 Tbit/s with a single comb laser. To further increase the data transmission bandwidth, an upgraded solution is proposed here by using four QD-CPMLs operated at separately adjusted temperatures. Over 36 nm wide comb spectrum with 100 GHz grid is obtained which can generate at least 60 comb lines for 4.8 Tbit/s transmission capacity.

To place our demonstration into context, the performance analyses of mode-locked comb lasers on various platforms have been compiled in Table 1. For external cavity MLLs, QW lasers exhibit relatively narrow optical linewidth, benefitting from their long cavity length [27–29]. But the repetition rates (comb spacings) are also limited within 20 GHz. In contrast, short-cavity two-section MLLs, which have a single saturable absorber at the end of the cavity, would be able to produce comb lines with larger channel spacing, but the optical linewidth is normally within the range of tens of megahertz [30–32]. In addition, high-repetition-rate two-section MLs do also experience low optical gain due to their short cavity property, which leads to a significant degradation in single-channel output power. Here, by incorporating the high-order CPM technique, we could generate a 100 GHz grid comb laser with ultra-wide optical bandwidth (11.5 nm), while retaining 1580 μm cavity length for sufficient output power.

2. DEVICE DESIGN AND FABRICATION

The epitaxy of the QD-CPML is grown by molecular beam epitaxy on an n-type GaAs (100) substrate, containing eight stacks of self-assembled InAs QD layers. The active region of the dots in well structure is p-doped to improve the high-temperature stability of the lasers. A symmetric cladding layer design is used by utilizing 1500 nm thick p-type and n-type $Al_{0.4}Ga_{0.6}As$ for upper and lower cladding layers, respectively. In order to achieve 100 GHz repetition rate, an ultra-short laser cavity length of approximately 400 μm is normally required, which encounters significant gain reduction issues limiting the maximum output power of individual comb lines. To remain sufficient gain area, while keeping large mode spacing, here we introduce a high-order CPML design to overcome the insufficient gain issue. The schematic of the fourth-order QD-CPML is shown in Fig. 1(a). The total distance of the laser cavity is 4 times longer than that of the two-section MLL which produces pulses with fundamental repetition rate. In order to produce 100 GHz spacing OFCs, the cavity length of the fundamental mode is calculated as ~395 μm by using an effective group index of 3.8. Considering that QD lasers with such a short cavity may not have enough gain to support stable mode locking and decent output power, a fourth-order MLL design with 1580 μm cavity length is implemented here to allow four colliding pulses traveling intracavity to produce fourth-order harmonic pulses at 100 GHz repetition rate. As shown in Fig. 1(a), three saturable absorbers (SAs) equally divide the entire laser cavity with four gain sections, while all the SAs and gain sections are electrically connected through probe metal layers to simplify the measurement. There has been a high-order harmonic design of two SAs applied in the front and rear of the laser facets [38], as we found the evenly distributed SAs could produce more stable high-order harmonic mode-locking combs. To suppress the losses induced from extra SAs included here, the overall length of three SAs is chosen as 10% of the

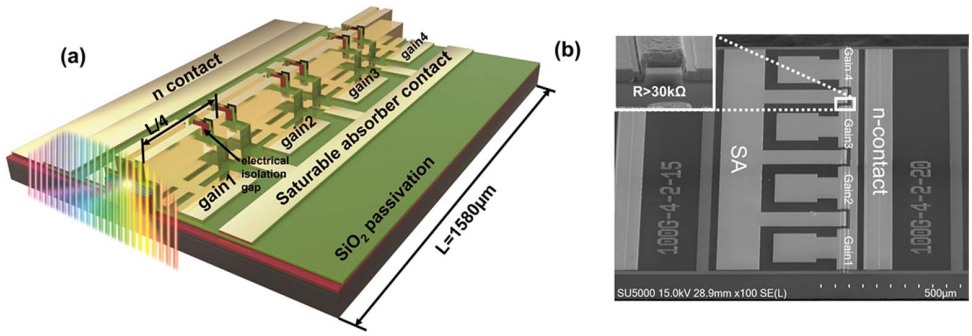

Fig. 1. (a) Schematic of InAs/GaAs fourth-order CPML design (total cavity length of 1580 μm) with four gain sections (360 μm for each section) and three equally spaced saturable absorbers (50 μm for each SA). (b) Cross-section SEM image of a fabricated device with a 45° tilted angle. Inset: magnified SEM image on electrical isolation trench region.

total cavity length, slightly shorter than the conventional design (usually 15%–20%).

The QD-CPMLs are fabricated with ridge waveguide and mesa widths of 4 μm and 25 μm, respectively. The three SAs are equally spaced along the cavity with the length of 50 μm, where the electrical isolation gap next to the SA is designed as 10 μm wide. The QD-CPML is then fabricated in line with the standard ridge waveguide InAs QD lasers by using dry etching, dielectric passivation, and metal contact deposition. The electrical isolation gaps are simultaneously defined with ridge waveguide etching by carefully controlling the dry etching depth at 100 nm above the active region. This process simply avoids additional efforts made to the definition of isolation trenches. The detailed fabrication processes are discussed in our previous work [23–25]. The SEM picture in Fig. 1(b) shows the fabricated QD-CPML device, where the inset shows the zoom-in isolation gap region between the gain section and the SA. The sheet resistance is ∼30 kΩ measured through *I-V* characteristics, which provides enough electrical isolation between SAs and gain sections. After device process, the laser die is mechanically thinned to 105 μm and cleaved into laser bars without high-reflection coating for this work.

3. DEVICE CHARACTERIZATIONS AND DISCUSSION

The fabricated QD-CPML is mounted on an AlN chip-on-carrier (CoC) for heat dissipation, while all the SAs, gain sections, and n contact pads are wire bonded to the CoC with three separated pads. The QD-CPML CoC is then mounted on top of a thermoelectric cooler for constant temperature control. The gain sections are driven by the Keithley 2520 current source and SAs are reverse biased by a voltage source. By using an integration sphere with an InGaAs photodetector to collect optical output power from lasers, the light-current (*L-I*) performance of the QD-CPML was characterized as shown in Fig. 2(a).

The lasers are characterized with gain current (I_g) ranging from 0 to 200 mA and SA reverse biased (V_{SA}) from 0 to −5 V under wide temperature variation from 20°C to 100°C. It shows that the QD-CPML could operate at a high temperature of 100°C and still exhibit optical power over 15 mW at condition $I_g = 200$ mA and $V_{SA} = 0$ V. Among all reverse bias conditions, the characteristic temperature is always larger than 110 K at temperatures from 20°C to 70°C. This temperature resilience performance is contributed to the p-doped active region of QD lasers [39,40]. At fixed temperature condition, the increment of reverse biased SA voltage causes the decreased optical output power and elevated threshold current. For example, at 20°C, as V_{SA} increased from 0 to −5 V, the optical power dropped from 32 to 28 mW. In addition, the threshold current increases slightly from 29 to 36 mA, which is mainly caused by the higher cavity losses induced from SAs. Noticeably, under reverse bias conditions, the *L-I* curve shows the abrupt kink around threshold, which is caused by the non-linear saturation effect of SAs [15,33]. These effects are enhanced at high reverse biased voltage ($V_{SA} = -5$ V) and high temperature operation (90°C) due to the strong absorption from SAs and simultaneous gain degradation at high temperature. Figure 2(b) shows the temperature-dependent optical spectral evolution of the QD-CPML from 20°C to 100°C at optimum operation conditions. The operation conditions marked at each temperature are slightly adjusted to achieve flat-top combs. It is noted that the 3 dB optical bandwidth does not dramatically narrow as the temperature increases, which indicates the stable operation of flat-top combs. Even at high temperature operation of 80°C, 3 dB bandwidth of 11.3 nm can still be achieved, which is the widest flat-top OFCs reported at high temperature to the best of our knowledge. The broadband comb source only starts to degrade at 100°C in line with the rolled-over *L-I* curves, in which case the laser can only generate 3.8 nm wide comb lines under optimized operation conditions. Interestingly, an ultra-flat comb spectrum with just 0.8 dB variation between 14 combs is achieved at 80°C. We suspect that this phenomenon is caused by ideal dispersion compensation at this specific operation point [41].

To investigate an optimum operation window of the fourth-order CPML where stable 100 GHz spacing flat-top OFCs can be generated, a wide range of operation conditions have been systematically mapped with I_g ranging from 50 to 250 mA and V_{SA} ranging from 0 to −5 V at room temperature. The 3 dB optical bandwidth and pulse width are characterized using an optical spectrum analyzer and autocorrelator (AC) in order to analyze the comb performance in the frequency and time domains, respectively. In order to characterize the 3 dB optical

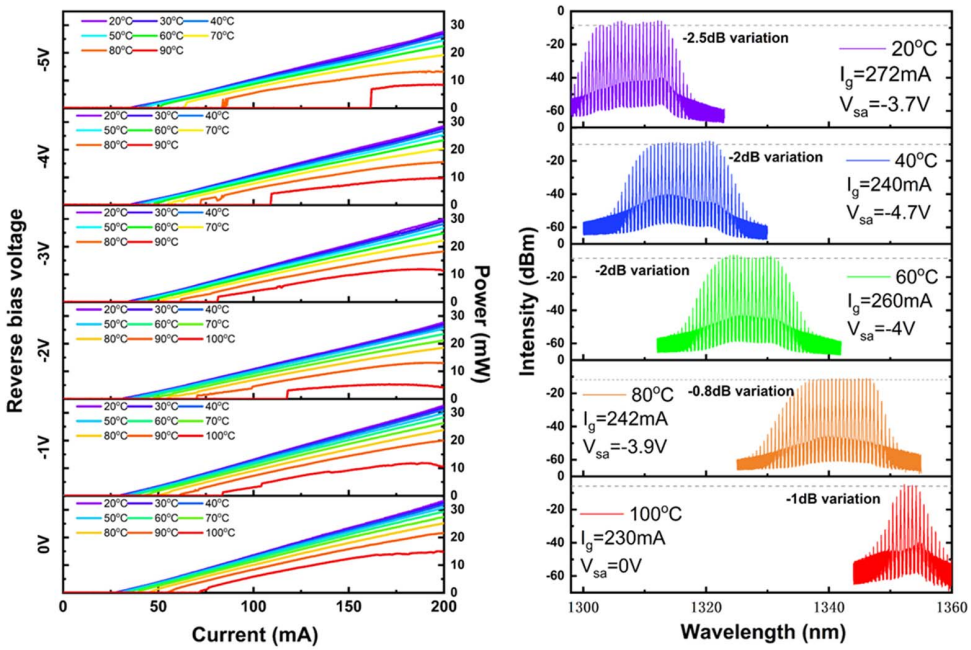

Fig. 2. (a) Temperature-dependent continuous-wave light current (*L-I*) characteristics of fourth-order QD-CPML from 20°C to 100°C under varied reverse bias voltages from 0 to −5 V. The kinks in *L-I* curves at high V_{SA} are induced from non-linear saturation effect of SAs. (b) Optical spectral evolutions with temperature increased from 20°C to 100°C. The operating current and reverse bias voltage at each temperature are slightly adjusted to achieve flat-top comb spectra.

bandwidth of the OFCs, optical spectral mapping under different operating conditions is studied in Fig. 3(a). In Fig. 3(a), as the gain section current increased, the single-comb spectral lobe started to split into dual-state operation. The spectral splitting may be caused by state filling [42] or spatial hole burning effect [43]; hence, photons excited by two groups of InAs QDs with different group velocity are formed inside the cavity, which leads to the dual-state mode-locked condition or unlocked region at low reverse bias. Simultaneous with the occurrence of the dual-state region, the AC pulse traces also disappear at this unlocked region. It is noted that the spectra have unstable regions (I_g = 150–160 mA, 190–200 mA) where random modes appear, that lead to uneven comb spacings. These unstable comb regions are marked as the gray area in Fig. 3(a), which is believed to be caused by strong mode competition within the dual-state region. Exceptionally, an ultra-wide optical comb spectrum is achieved at 180 mA (V_{SA} = −3 V) by perfect merging of two lobes of comb lines; however, the operation window is relatively narrow comparing to the stable flat-top comb region at higher injection current. Therefore, by further increasing the injection current and reverse bias voltage, we have reached a flat-top region above 210 mA, where the 3 dB bandwidth significantly broadened. This region is here defined as the optimum operation range of the QD-CPML for an ultra-broadband flat-top comb source.

The generation of broadband flat-top combs is the major focus in this paper for high-capacity WDM applications. For the flat-top ML region discussed above, a high-resolution sweep of comb line counts within 3 dB optical bandwidth is performed over an optimum reverse bias range from 3 to 4.5 V with magnified 0.1 V step and varying injection current from 210 to 250 mA under 1 mA step increment. As shown in Fig. 3(b), there is a "riverway"-like unlocked region separating the flat-top comb area; along the left "riverbank," the comb spectral bandwidth reaches the maximum condition. Two dark red blocks show the best conditions which can generate 20 comb lines within the 3 dB optical bandwidth.

Three operation zones are distinguished here by analyzing the spectral envelope shapes, which are the single-state region, dual-state region, and flat-top region. In addition, the mapping results of pulse width are shown in Fig. 3(c), where the narrowest full width at half-maximum of AC trace (dark red region) is ∼810 fs at the operating condition V_{SA} = −2 V, I_g = 100–120 mA, which is comparable to the state-of-the-art performance of two-section MLLs [30,32]. No AC pulses or very weak pulses are observed in the gray area of the mapping; hence this operating condition is defined as the unlocked region. Furthermore, the time–bandwidth product (TBP) values are then calculated and mapped in Fig. 3(d) using the data shown in Figs. 3(a) and 3(c). In the single-state ML region, the TBP value is normally below 1.2, except that very small TBP value of ∼0.45 is achieved at 120 mA, which is close to the Gaussian shape Fourier transfer limited theoretical value of 0.44. This Fourier transfer limited region is marked in Fig. 3(c).

As injection currents are elevated over 210 mA, the dual-state region was strongly suppressed, while merging back into single-lobe comb spectra as shown in Fig. 3(e). Different from the Gaussian-shape-like spectrum, the optical spectrum is broadened to a rectangular shape with flat profiles, and thus the region is named as flat-top ML. The formation of the flat-top profile is induced from the great compensation of increased Kerr non-linearity at high carrier injection toward

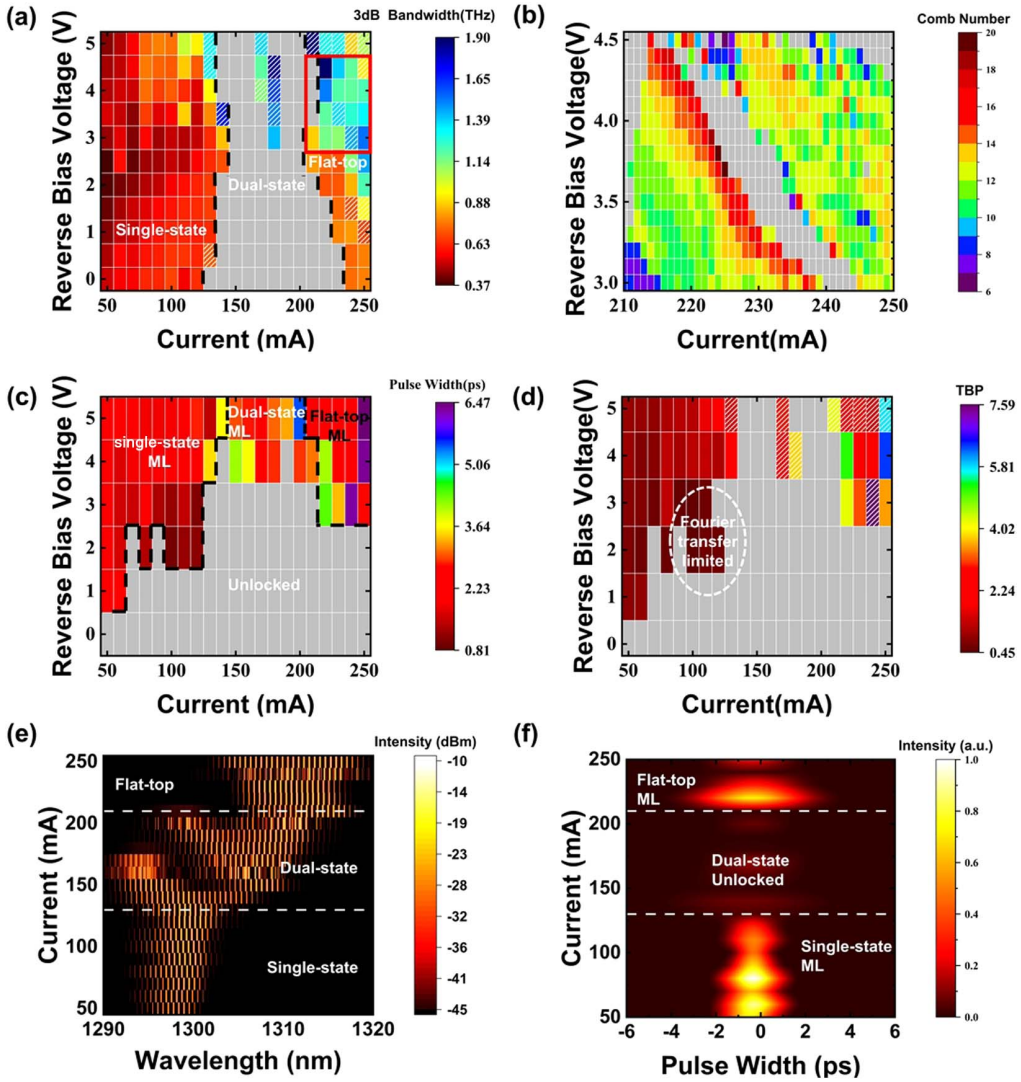

Fig. 3. Fourth-order QD-CPML. (a) Optical spectrum 3 dB bandwidth mapping as a function of SA reverse bias voltage ranging from 0 to 5 V with 0.5 V step and injection current of gain sections varying from 50 to 250 mA with 10 mA step. (b) A precisely swept map of comb line numbers within 3 dB optical bandwidth as a function of SA reverse bias voltage varying from 3 to 4.5 V with 0.1 V step and gain section injection current changing from 210 to 250 mA with 1 mA step [the mapping area corresponds to the red rectangular zone in (a)]. (c) Pulse width and (d) time–bandwidth product (TBP) mapping as a function of SA reverse bias voltage ranging from 0 to 5 V with 1 V step and gain section injection current ranging from 50 to 250 mA with 10 mA step. (e) Optical spectra and (f) pulse AC trace evolutions with injection current from 50 to 250 mA with 10 mA step at −3 V reverse bias voltage.

increased group velocity dispersion (GVD) across the enlarged spectral bandwidth. Similar mechanisms have been previously discussed theoretically and experimentally in single-section MLLs [44–47]. The results are in line with significantly broadened AC pulse width of a few picoseconds [Fig. 3(c)], indicating an enhanced dispersion process within the flat-top MLL region compared with the single-state MLL region.

To further investigate the ML evolution at fixed reverse bias voltage in both optical spectral and time domains, current dependent optical spectral and normalized pulse width evolutions at $V_{SA} = -3$ V are plotted in Figs. 3(e) and 3(f), respectively. Right above the threshold current, the QD-CPML operates as a single-state comb spectrum at the injection current ranging from 50 to 120 mA, where the optical spectra are redshifted and broadened with increased current, eventually moving into the flat-top region above 210 mA. In the time domain [Fig. 3(f)], the pulses are getting narrower toward the injection current of 120 mA, where the sub-picosecond pulse of 860 fs is detected. Further into the flat-top ML region, due to increased GVD, the pulse width is also extended to few picoseconds. Overall, the optical spectral mapping, pulse width mapping, and TBP mapping are in good agreement, which gives us clear guidance in operation condition selection for different application scenarios.

Under the optimum operating condition of $I_g = 224$ mA and $V_{SA} = -3.8$ V, twenty 100 GHz spacing comb channels with 3 dB optical bandwidth of 11.5 nm are produced, as shown in Fig. 4(a). It can be clearly observed that each comb

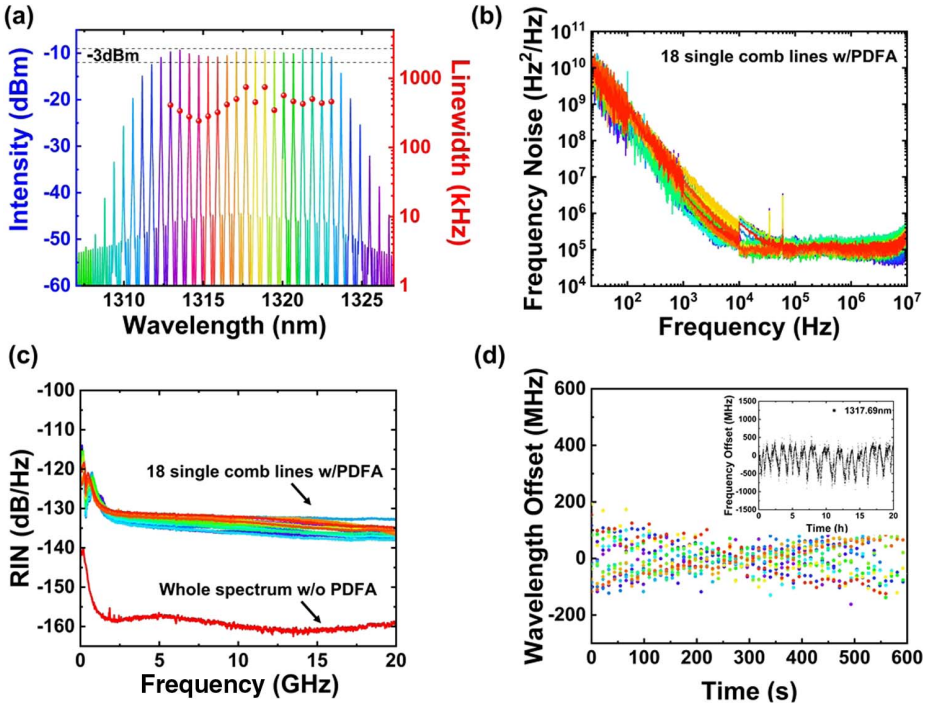

Fig. 4. (a) Optical spectrum of flat-top QD-CPML under optimized bias condition of $I_g = 224$ mA and $V_{SA} = -3.8$ V. (b) Optical linewidth of the frequency noise spectra from 18 filtered comb lines. (c) Relative intensity noise (RIN) of 18 filtered individual comb lines and the whole laser. (d) Wavelength stability of 18 comb lines over 10 min and a single comb line wavelength offset over 20 h (inset). (b), (c), and (d) are characterized at the same set of operating conditions as in (a).

line exhibits optical signal-to-noise ratio over 35 dB. To examine the performance of each comb channel, a tunable bandpass filter (EXFO XTM-50) is used together with an O-band praseodymium-doped fiber amplifier (PDFA) (FiberLabs Inc. AMP-FL8611-OB-16) for overcoming the coupling and insertion loss. To note, the measured single-channel optical power is approximately 1.7 mW without taking into account the coupling loss and insertion loss from the optical bandpass filter (OBPF) (before coupling into the OBPF). The frequency noise is characterized through a commercial homodyne system (OEwave 4000).

Figure 4(b) shows the frequency noise spectra of 18 filtered comb lines. By fitting the white noises, the intrinsic Lorentz optical linewidths are estimated and plotted in Fig. 4(a). The average optical linewidth of 18 comb channels is approximately 440 kHz, which is 1 order of magnitude lower than that of the reported conventional QD MLLs [30]. The narrow optical linewidth indicates that the phases of individual comb lines are highly coherent through high-order mode locking. Furthermore, the relative intensity noise (RIN) spectra of each comb line (PDFA amplified) and entire comb spectrum are both characterized. Figure 4(c) shows that the 18 individual channels and whole comb spectrum have average RINs of −135 dB/Hz and −160 dB/Hz in the range from 0 to 20 GHz, respectively. Although there is approximately 25 dB/Hz degradation in RIN values for individual comb lines, the average RIN values of each single sideband still meet the requirements for high-speed PAM-4 modulation [48] and WDM standards [36]. Moreover, the stability of each comb channel is tested using a wavelength meter (Thorlabs OSA 202C) in Fig. 4(d). The wavelength drift of 18 combs is less than 200 MHz for 10 min monitoring. For the extended time stability test that is also applied to a comb channel at 1317.69 nm, the wavelength variation is less than 1 GHz, as shown in the inset of Fig. 4(d). All the measurements are under free-running conditions, and it is believed that the combs can be further stabilized by the wavelength locker design with a feedback control loop [14].

High-speed external modulation of the fourth-order CPML is demonstrated by evaluating the eye diagram performance of the laser. The large signal modulation experimental setup for the QD comb laser is shown in Fig. 5(a). The CPML is operated at optimum flat-top conditions as discussed above, then coupled into an OBPF to select individual comb channels as optical carriers. A single channel at 1321.28 nm is selected for testing to show the typical performance. By adjusting the amplification current of the PDFA, the carrier is amplified to 10 dBm and coupled into a 40 GHz lithium niobate (LN) Mach–Zehnder modulator (iXblue MX1300-LN-40) for data modulation. The modulation signals are produced from an arbitrary waveform generator (Keysight M8194A) with a $2^7 - 1$ pseudo-random binary sequence patterns. The signals are amplified to ∼3 V peak-to-peak output power through a 38 GHz broadband RF amplifier (SHF 806E). The external modulated signals are then sent to an optical sampling oscilloscope (Tektronix DSA8300) to show the eye diagram. Figures 5(b) and 5(c) show the measured eye diagrams for 70 Gbit/s NRZ and 40 GBaud/s PAM-4 modulation formats

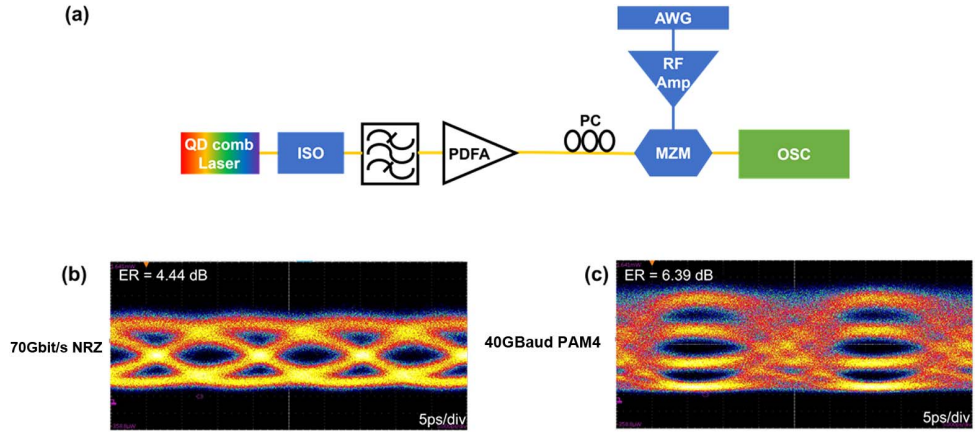

Fig. 5. (a) Experimental setup used to measure B2B NRZ and PAM-4 transmission characteristics of QD-CPML, including ISO, optical isolator; OBPF, optical bandpass filter; PDFA, praseodymium-doped fiber amplifier; PC, polarization controller; AWG, arbitrary waveform generator; RF Amp, RF amplifier; MZM, Mach–Zehnder modulator; OSC, optical sampling oscilloscope. (b) 70 Gbit/s NRZ and (c) 40 GBaud PAM-4 optical eye diagram using comb line at 1321.28 nm.

with extinction ratios of 4.4 dB and 6.4 dB, respectively. To note, the modulation speed used here is limited by the maximum bandwidth of the O-band LN modulator, which is expected to reach over 100 Gbit/s with additional advanced digital signal process [30] and large bandwidth EO modulator [49]. Here, all comb channels have been measured through high-speed modulation, which exhibit similar eye diagrams at 80 Gbit/s. Since there are 20 channels in total within the 3 dB optical bandwidth, the 100 GHz spacing flat-top OFC can be practically used to achieve 1.6 Tbit/s data transmission using the 40 GBaud/s PAM-4 modulation format.

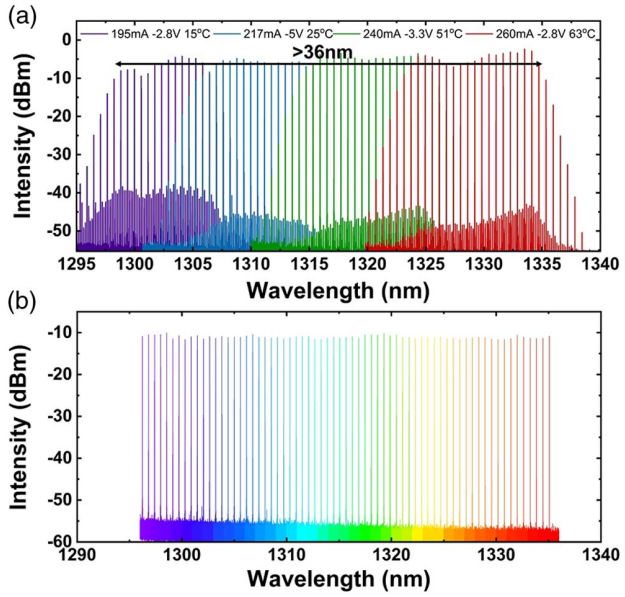

Fig. 6. (a) Combined optical spectra of fourth-order QD-CPML for extended optical bandwidth under the temperatures of 15°C, 25°C, 51°C, and 63°C (purple line: $I_g = 195$ mA, $V_{SA} = -2.8$ V; blue line: $I_g = 217$ mA, $V_{SA} = -5$ V; green line: $I_g = 240$ mA, $V_{SA} = -3.3$ V; red line: $I_g = 260$ mA, $V_{SA} = -2.8$ V). The maximum channel counts can reach 60 comb lines within 6 dB optical bandwidth. (b) Combined optical spectra of all 60 channels with filtering of each channel via the OBPF.

The total transmission bandwidth can also be enhanced in the aspect of optical bandwidth. Taking advantage of the temperature resilience properties of QD lasers, the optical spectrum could be extended by combining the output optical spectra from the QD laser array where each laser is operated at properly designed temperature. The proof-of-concept experiment has been performed by adjusting the operation temperature of a QD-CPML to seamlessly combine and extend the optical spectra. As shown in Fig. 6, the 6 dB optical bandwidth of OFCs is successfully extended to 36 nm with temperature varying from 15°C to 63°C. The broadened optical bandwidth includes sixty 100 GHz spacing OFCs, which has the potential of increasing the data transmission capacity further to 4.8 Tbit/s.

4. CONCLUSIONS

We have successfully demonstrated an O-band 100 GHz grid fourth-order QD-CPML with a record high 3 dB optical bandwidth of 11.5 nm. Taking advantage of the temperature insensitivity of QDs, the laser could generate flat-top OFCs with average 3 dB bandwidth over 10 nm within a wide temperature range from 20°C to 80°C. Sophisticated analyses of high-order CPMLs are included in this work; both Fourier transfer limited sub-picosecond pulses and flat-top comb can be generated from the QD-CPML at different ML regions. The flat-top comb laser shows excellent integrated average RIN values of the entire spectrum and 18 filtered channels at −135 dB/Hz and −160 dB/Hz, respectively. We have achieved 18 flat-top comb lines with an average optical linewidth of 440 kHz, which is the lowest value for high-order CPM semiconductor lasers to the best of our knowledge. Without active feedback loop control, the free-running QD-CPML has a wavelength offset value less than 1 GHz over 20 h reliability test. Twenty comb lines are selected as optical carriers with 1.6 Tbit/s transmission capability being demonstrated by modulating each channel with 40 GBaud/s PAM-4 format. An extended optical bandwidth solution is proposed here with 36 nm broadband spectrum

containing maximum 60 channels at 100 GHz grid, which is a promising approach to achieve 4.8 Tbit/s data transmission. As a weight and power multi-wavelength source solution, we expect this high-bandwidth flat-top QD-CPML would be widely used in WDM systems, optical interconnects, and photonic neural networks.

Funding. National Key Research and Development Program of China (2021YFB2800400); Youth Innovation Promotion Association of the Chinese Academy of Sciences (2018011); National Natural Science Foundation of China (61975230, 62008308).

Acknowledgment. The authors would like to thank Mr. Mingchen Guo, Miss Shujie Pan, and Miss Yiou Cui for their constructive contributions in device fabrications and measurements.

Disclosures. The authors declare no conflicts of interest.

Data Availability. Data underlying the results presented in this paper are not publicly available at this time but may be obtained from the authors upon reasonable request.

[†]These authors contributed equally to this paper.

REFERENCES

1. R. Wu, V. R. Supradeepa, C. M. Long, D. E. Leaird, and A. M. Weiner, "Generation of very flat optical frequency combs from continuous-wave lasers using cascaded intensity and phase modulators driven by tailored radio frequency waveforms," Opt. Lett. **35**, 3234–3236 (2010).
2. M. Y. Xu, M. B. He, Y. T. Zhu, S. Y. Yu, and X. L. Cai, "Flat optical frequency comb generator based on integrated lithium niobate modulators," J. Lightwave Technol. **40**, 339–345 (2021).
3. S. Liu, K. Wu, L. Zhou, L. Lu, B. Zhang, G. Zhou, and J. Chen, "Optical frequency comb and Nyquist pulse generation with integrated silicon modulators," IEEE J. Sel. Top. Quantum Electron. **26**, 8300208 (2019).
4. P. Delhaye, A. Schliesser, O. Arcizet, T. Wilken, R. Holzwarth, and T. J. Kippenberg, "Optical frequency comb generation from a monolithic microresonator," Nature **450**, 1214–1217 (2007).
5. T. J. Kippenberg, R. Holzwarth, and S. A. Diddams, "Microresonator-based optical frequency combs," Science **332**, 555–559 (2011).
6. M. G. Suh and K. J. Vahala, "Soliton microcomb range measurement," Science **359**, 884–887 (2018).
7. W. L. Weng, A. Kaszubowska-Anandarajah, J. J. He, P. D. Lakshmijayasimha, E. Lucas, J. Q. Liu, P. M. Anandarajah, and T. J. Kippenberg, "Gain-switched semiconductor laser driven soliton microcombs," Nat. Commun. **12**, 1425 (2021).
8. R. Zhou, S. Latkowski, J. O'Carroll, R. Phelan, L. P. Barry, and P. Anandarajah, "40 nm wavelength tunable gain-switched optical comb source," Opt. Express **19**, B415–B420 (2011).
9. E. U. Rafailov, M. A. Cataluna, and W. Sibbett, "Mode-locked quantum-dot lasers," Nat. Photonics **1**, 395–401 (2007).
10. A. Aboketaf, A. Elshaari, and S. Preble, "Optical time division multiplexer on silicon chip," Opt. Express **18**, 13529–13535 (2010).
11. D. Kong, H. Xin, K. Kim, Y. Liu, L. K. Oxenloewe, P. Dong, and H. Hu, "Intra-datacenter interconnects with a serialized silicon optical frequency comb modulator," J. Lightwave Technol. **38**, 4677–4682 (2020).
12. Z. Lu, J. Liu, S. Raymond, P. Poole, P. Barrios, and D. Poitras, "312-fs pulse generation from a passive C-band InAs/InP quantum dot mode-locked laser," Opt. Express **16**, 10835–10840 (2008).
13. J. Liu, Z. Lu, S. Raymond, P. Poole, P. Barrios, and D. Poitras, "Dual-wavelength 92.5 GHz self-mode-locked InP-based quantum dot laser," Opt. Lett. **33**, 1702–1704 (2008).
14. Z. G. Lu, J. R. Liu, C. Y. Song, J. Weber, Y. Mao, S. D. Chang, H. P. Ding, P. J. Poole, P. J. Barrios, D. Poitras, S. Janz, and M. O'Sullivan, "High performance InAs/InP quantum dot 34.462-GHz C-band coherent comb laser module," Opt. Express **26**, 2160–2167 (2018).
15. X. Huang, A. Stintz, H. Li, L. F. Lester, J. Cheng, and K. J. Malloy, "Passive mode-locking in 1.3 μm two-section InAs quantum dot lasers," Appl. Phys. Lett. **78**, 2825–2827 (2001).
16. B. Dong, H. Huang, J. Duan, G. Kurczveil, D. Liang, R. Beausoleil, and F. Grillot, "Frequency comb dynamics of a 1.3 μm hybrid-silicon quantum dot semiconductor laser with optical injection," Opt. Lett. **44**, 5755–5758 (2019).
17. J. Duan, H. Huang, B. Dong, J. C. Norman, Z. Zhang, J. E. Bowers, and F. Grillot, "Dynamic and nonlinear properties of epitaxial quantum dot lasers on silicon for isolator-free integration," Photon. Res. **7**, 1222–1228 (2019).
18. J. J. Chen, Z. H. Wang, W. Q. Wei, T. Wang, and J. J. Zhang, "Sole excited-state InAs quantum dot laser on silicon with strong feedback resistance," Front. Mater. **8**, 163 (2021).
19. J. Kwoen, B. Jang, K. Watanabe, and Y. Arakawa, "High-temperature continuous-wave operation of directly grown InAs/GaAs quantum dot lasers on on-axis Si (001)," Opt. Express **27**, 2681–2688 (2019).
20. J. C. Norman, D. Jung, Z. Y. Zhang, Y. T. Wang, S. T. Liu, C. Shang, R. W. Herrick, W. W. Chow, A. C. Gossard, and J. E. Bowers, "A review of high-performance quantum dot lasers on silicon," IEEE J. Quantum Electron. **55**, 2000511 (2019).
21. S. Chen, W. Li, J. Wu, Q. Jiang, M. Tang, S. Shutts, S. N. Elliott, A. Sobiesierski, A. J. Seeds, I. Ross, and P. M. Smowton, "Electrically pumped continuous-wave III–V quantum dot lasers on silicon," Nat. Photonics **10**, 307–311 (2016).
22. A. Y. Liu, C. Zhang, J. Norman, A. Snyder, D. Lubyshev, J. M. Fastenau, A. W. Liu, A. C. Gossard, and J. E. Bowers, "High performance continuous wave 1.3 μm quantum dot lasers on silicon," Appl. Phys. Lett. **104**, 041104 (2014).
23. Z. H. Wang, W. Q. Wei, Q. Feng, T. Wang, and J. J. Zhang, "InAs/GaAs quantum dot single-section mode-locked lasers on Si (001) with optical self-injection feedback," Opt. Express **29**, 674–683 (2021).
24. W. Q. Wei, J. Y. Zhang, J. H. Wang, H. Cong, J. J. Guo, Z. H. Wang, H. X. Xu, T. Wang, and J. J. Zhang, "Phosphorus-free 1.5 μm InAs quantum-dot microdisk lasers on metamorphic InGaAs/SOI platform," Opt. Lett. **45**, 2042–2045 (2020).
25. W. Q. Wei, Q. Feng, J. J. Guo, M. C. Guo, J. H. Wang, Z. H. Wang, T. Wang, and J. J. Zhang, "InAs/GaAs quantum dot narrow ridge lasers epitaxially grown on SOI substrates for silicon photonic integration," Opt. Express **28**, 26555–26563 (2020).
26. Q. Feng, W. Q. Wei, B. Zhang, H. L. Wang, J. H. Wang, H. Cong, T. Wang, and J. J. Zhang, "O-band and C/L-band III-V quantum dot lasers monolithically grown on Ge and Si substrate," Appl. Sci. **9**, 385 (2019).
27. Z. C. Wang, K. V. Gasse, V. Moskalenko, S. Latkowski, E. Bente, B. Kuyken, and G. Roelkens, "A III-V-on-Si ultra-dense comb laser," Light Sci. Appl. **6**, 6260 (2017).
28. V. Corral, R. Guzmán, C. Gordón, X. J. M. Leijtens, and G. Carpintero, "Optical frequency comb generator based on a monolithically integrated passive mode-locked ring laser with a Mach–Zehnder interferometer," Opt. Lett. **41**, 1937–1940 (2016).
29. M. L. Davenport, S. T. Liu, and J. E. Bowers, "Integrated heterogeneous silicon/III–V mode-locked lasers," Photon. Res. **6**, 468–478 (2018).
30. S. T. Liu, X. R. Wu, D. Jung, J. C. Norman, M. J. Kennedy, H. K. Tsang, A. C. Gossard, and J. E. Bowers, "High-channel-count 20 GHz passively mode-locked quantum dot laser directly grown on Si with 4.1 Tbit/s transmission capacity," Optica **6**, 128–134 (2019).
31. S. J. Pan, J. O. Huang, Z. C. Zhou, Z. X. Liu, L. Ponnampalam, Z. Z. Liu, M. C. Tang, M. C. Lo, Z. Z. Cao, K. Nishi, K. Takemasa, M. Sugawara, R. Penty, I. White, A. Seeds, H. Y. Liu, and S. M. Chen, "Quantum dot mode-locked frequency comb with ultra-stable 25.5 GHz spacing between 20°C and 120°C," Photon. Res. **8**, 1937–1942 (2020).

32. L. P. Hou, Y. G. Huang, Y. H. Liu, R. K. Zhang, J. K. Wang, B. J. Wang, H. L. Zhu, B. Hou, B. C. Qiu, and J. H. Marsh, "Frequency comb with 100 GHz spacing generated by an asymmetric MQW passively mode-locked laser," Opt. Lett. **45**, 2760–2763 (2020).
33. G. Kurczveil, C. Zhang, A. Descos, D. Liang, M. Fiorentino, and R. Beausoleil, "On-chip hybrid silicon quantum dot comb laser with 14 error-free channels," in *IEEE International Semiconductor Laser Conference (ISLC)* (2018), pp. 1–2.
34. G. Kurczveil, A. Descos, D. Liang, M. Fiorentino, and R. Beausoleil, "Hybrid silicon quantum dot comb laser with record wide comb width," in *OSA FiO_LS Virtual Conference* (2020), paper FTu6E.6.
35. C. Kumar and R. Goyal, "Effect of crosstalk in super dense wavelength division multiplexing system using hybrid optical amplifier," J. Opt. Commun. **40**, 347–351 (2019).
36. M. Sysak, J. Johnson, and D. Lewis, "CW-WDM MSA technical specifications Rev 1.0," CW-WDM MSA public document (2021).
37. Z. Zhang, R. Hogg, X. Lv, and Z. Wang, "Self-assembled quantum-dot superluminescent light-emitting diodes," Adv. Opt. Photonics **2**, 201–228 (2010).
38. Y. Li, F. Chiragh, Y. Xin, C. Lin, J. Kim, C. Christodoulou, and L. Lester, "Harmonic mode-locking using the double interval technique in quantum dot lasers," Opt. Express **18**, 14637–14643 (2010).
39. H. Y. Liu, S. L. Liew, T. Badcock, D. J. Mowbray, M. S. Skolnick, S. K. Ray, T. L. Choi, K. M. Groom, B. Stevens, F. Hasbullah, and C. Y. Jin, "P-doped 1.3 μm InAs/GaAs quantum-dot laser with a low threshold current density and high differential efficiency," Appl. Phys. Lett. **89**, 073113 (2006).
40. J. Z. Huang, W. Q. Wei, J. J. Chen, Z. H. Wang, T. Wang, and J. J. Zhang, "P-doped 1300 nm InAs/GaAs quantum dot lasers directly grown on SOI substrate," Opt. Lett. **46**, 5525–5528 (2021).
41. J. K. Mee, R. Raghunathan, D. Murrell, A. Braga, Y. Li, and L. F. Lester, "Novel optical systems design and optimization XVII," Proc. SPIE **9193**, 919301 (2014).
42. S. G. Li, Q. Y. Gong, Y. F. Lao, H. Yang, S. Gao, P. Chen, Y. G. Zhang, S. L. Feng, and H. L. Wang, "Two-color quantum dot laser with tunable wavelength gap," Appl. Phys. Lett. **95**, 251111 (2009).
43. M. Charis, C. Simos, I. Simos, S. Mikroulis, I. Krestnikov, and D. Syvridis, "Pulse width narrowing due to dual ground state emission in quantum dot passively mode locked lasers," Appl. Phys. Lett. **96**, 211110 (2010).
44. J. Hillbrand, D. Auth, M. Piccardo, N. Opačak, E. Gornik, G. Strasser, F. Capasso, S. Breuer, and B. Schwarz, "In-phase and anti-phase synchronization in a laser frequency comb," Phys. Rev. Lett. **124**, 023901 (2020).
45. N. Opačak and B. Schwarz, "Theory of frequency-modulated combs in lasers with spatial hole burning, dispersion, and Kerr nonlinearity," Phys. Rev. Lett. **123**, 243902 (2019).
46. S. P. Duill, S. G. Murdoch, R. T. Watts, R. Rosales, A. Ramdane, P. Landais, and L. P. Barry, "Simple dispersion estimate for single-section quantum-dash and quantum-dot mode-locked laser diodes," Opt. Lett. **41**, 5676–5679 (2016).
47. R. Rosales, S. G. Murdoch, R. T. Watts, K. Merghem, A. Martinez, F. Lelarge, A. Accard, L. P. Barry, and A. Ramdane, "High performance mode locking characteristics of single section quantum dash lasers," Opt. Express **20**, 8649–8657 (2012).
48. N. Eiselt, H. Griesser, M. Eiselt, W. Kaiser, S. Aramideh, J. Olmos, I. Monroy, and J. Elbers, "Real-time 200 Gb/s (4 × 56.25 Gb/s) PAM-4 transmission over 80 km SSMF using quantum-dot laser and silicon ring-modulator," in *Optical Fiber Communication Conference* (2017), Vol. **Part F40-O**, paper W4D.3.
49. M. B. He, M. Y. Xu, Y. X. Ren, J. Jian, Z. L. Ruan, Y. S. Xu, S. Q. Gao, S. H. Sun, X. Q. Wen, L. D. Zhou, L. Liu, C. J. Guo, H. Chen, S. Y. Yu, L. Liu, and X. L. Cai, "High-performance hybrid silicon and lithium niobate Mach–Zehnder modulators for 100 Gbit s^{-1} and beyond," Nat. Photonics **13**, 359–364 (2019).